Nuclear Engineering and Technology 55 (2023) 4491–4503

Contents lists available at ScienceDirect

Nuclear Engineering and Technology

journal homepage: www.elsevier.com/locate/net

Original Article

CEFR control rod drop transient simulation using RAST-F code system

Tuan Quoc Tran [a], Xingkai Huo [b], Emil Fridman [c], Deokjung Lee [a,d,*]

[a] Department of Nuclear Engineering, Ulsan National Institute of Science and Technology, 50 UNIST-gil, Ulsan, 44919, Republic of Korea
[b] China Institute of Atomic Energy, POB 275(95), Beijing, 102413, China
[c] Helmholtz-Zentrum Dresden-Rossendorf, Bautzner Landstraße 400, 01328, Dresden, Germany
[d] Advanced Nuclear Technology and Services, 406-21 Jonga-ro, Jung-gu, Ulsan, 44429, Republic of Korea

ARTICLE INFO

Keywords:
CEFR
RAST-F
Transient
Nodal diffusion code
Serpent

ABSTRACT

This study aimed to verify and validate the transient simulation capability of the hybrid code system RAST-F for fast reactor analysis. For this purpose, control rod (CR) drop experiments involving eight separate CRs and six CR groups in the China Experimental Fast Reactor (CEFR) start-up tests were utilized to simulate the CR drop transient. The RAST-F numerical solution, including the neutron population, time-dependent reactivity, and CR worth, was compared against the measurement values obtained from two out-of-core detectors. Moreover, the time-dependent reactivity and CR worth from RAST-F were verified against the results obtained by the Monte Carlo code Serpent using continuous energy nuclear data. A code-to-code comparison between Serpent and RAST-F showed good agreement in terms of time-dependent reactivity and CR worth. The discrepancy was less than 160 pcm for reactivity and less than 110 pcm for CR worth. RAST-F solution was almost identical to the measurement data in terms of neutron population and reactivity. All the calculated CR worth results agreed with experimental results within two standard deviations of experimental uncertainty for all CRs and CR groups. This work demonstrates that the RAST-F code system can be a potential tool for analyzing time-dependent phenomena in fast reactors.

1. Introduction

The China Experimental Fast Reactor (CEFR) is a fast reactor (FR) located at the China Institute of Atomic Energy (CIAE) in Beijing, China. It is a sodium-cooled (FR) with a small core size (the active core height is 45 cm and the core radius is approximately 45 cm). It operates using 64.4 % high-enriched uranium (HEU) fuel. Its construction begun in 2000, and the first criticality was reached in July 2010. The commissioning work of the CEFR included a pre-operation test phase, charging, initial criticality, a low-power test phase, and a power test phase. A four-year coordinated research project (CRP) to develop CEFR benchmarks based on the start-up tests was proposed by the CIAE and International Atomic Energy Agency (IAEA) in 2018. Information regarding reactor core configuration, material, geometry, and experimental data is collected in benchmark packages for validation of neutronic codes. The fuel loading process, control rod (CR) worth measurement, reactivity effects such as temperature, fuel sub-assembly swap, sodium void measurements, and neutron reaction rate distribution measurement are included in the benchmark. At the end of the CRP, essential information and measurement data of CR drop transient experiments were additionally provided to all participants [1]. These data are important for validating the transient simulation capability of nuclear reactor simulation codes.

Recently, the COmputational Reactor physics and Experiment (CORE) laboratory of the Ulsan National Institute of Science and Technology (UNIST) has been working on developing tools for the Vodo-Vodyanoi Energeticheskiy Reactor (VVER) and FR design and analysis. The conventional two-step approach code system STREAM-V/RAST-V has been developed for VVER analysis, and initial studies have been conducted [2–4]. Meanwhile, a hybrid two-step approach code system MCS/RAST-F is under development for FR analysis that couples a multi-group cross-section (XS) generation Monte Carlo (MC) code MCS [5] and a multi-group nodal diffusion code RAST-F [6]. The code comprises specialized modules for FR analysis, including XS parameterization, thermal-hydraulic, microscopic XS depletion, and control sub-assembly movement modules. The triangle-based polynomial expansion nodal (TPEN) algorithm [7,8] has been implemented in RAST-F for solving 3D multi-group neutron diffusion equations based on the triangular-z mesh. The depletion calculation is performed by solving the transmutation equation using the Chebyshev Rational

* Corresponding author. Department of Nuclear Engineering, Ulsan National Institute of Science and Technology, 50 UNIST-gil, Ulsan, 44919, Republic of Korea.
E-mail address: deokjung@unist.ac.kr (D. Lee).

https://doi.org/10.1016/j.net.2023.08.017
Received 5 May 2023; Received in revised form 4 August 2023; Accepted 9 August 2023
Available online 10 August 2023

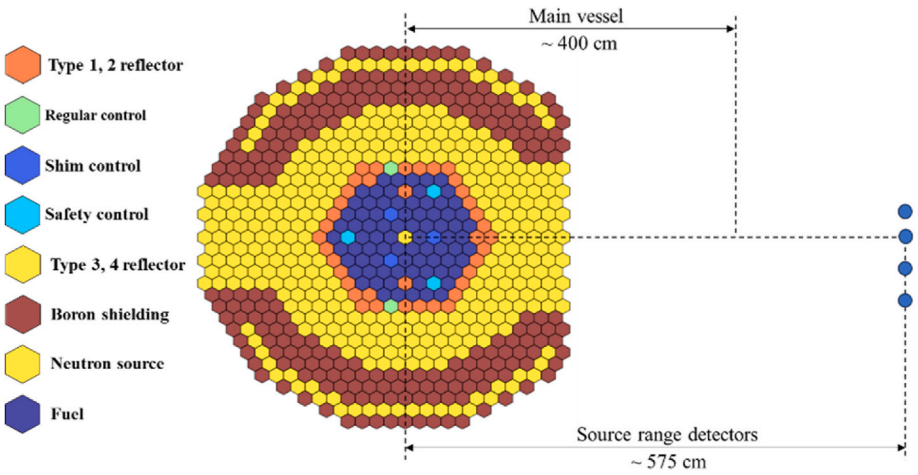

Fig. 1. Core configuration at operating load.

Table 1
Control sub-assembly positions and insertion duration.

CR/CR group	Core state	Control sub-assembly positions from the bottom of the fuel region [mm]								Drop duration (sec)
		RE1	RE2	SH1	SH2	SH3	SA1	SA2	SA3	
RE1	Initial	501	106	240	240	239	498	500	500	≤2.5
	Rodded	−1	106	240	240	239	498	500	500	
RE2	Initial	106	499	240	240	239	498	500	500	≤2.5
	Rodded	106	5	240	240	239	498	500	500	
SH1	Initial	240	240	501	141	141	498	499	499	≤2.5
	Rodded	240	240	4	141	141	498	499	499	
SH2	Initial	239	240	151	498	151	498	500	500	≤2.5
	Rodded	239	240	151	−1	151	498	500	500	
SH3	Initial	240	239	148	150	498	498	500	500	≤2.5
	Rodded	240	239	148	150	7	498	500	500	
SA1	Initial	240	239	240	240	241	498	499	499	≤0.7
	Rodded	240	239	240	240	241	46	499	499	
SA2	Initial	240	240	240	240	240	498	499	499	≤0.7
	Rodded	240	239	240	240	240	498	55	499	
SA3	Initial	240	239	240	240	240	498	499	499	≤0.7
	Rodded	240	239	240	240	240	498	499	40	
3 × SH+2 × RE	Initial	247	247	239	240	239	498	500	499	≤2.5
	Rodded	0	5	1	−1	7	498	500	499	
SH2+SH3+2 × RE	Initial	247	248	501	141	141	498	500	499	≤2.5
	Rodded	−2	2	501	−3	16	498	500	499	
3 × SA	Initial	247	249	240	240	240	498	500	499	≤0.7
	Rodded	247	249	240	240	240	46	56	40	
SA1+SA2	Initial	247	248	240	240	240	498	500	500	≤0.7
	Rodded	247	248	240	240	240	45	54	500	
2 × RE+3 × SH+3 × SA	Initial	247	248	240	240	240	499	500	500	≤2.5
	Rodded	0	3	2	−2	0	45	56	40	
2 × RE + SH2+SH3+3 × SA	Initial	248	248	500	141	141	498	500	499	≤2.5
	Rodded	−2	2	500	−3	7	45	55	40	

Table 2
Point kinetic data used for reactivity calculations.

Group	β_i [10^{-2}]	λ [s^{-1}]
1	0.0260	0.0127
2	0.1496	0.0317
3	0.1346	0.1151
4	0.2938	0.3111
5	0.0988	1.4001
6	0.0219	3.8713
β_{eff} [10^{-2}]	0.7247	–

Approximation Method (CRAM) [9], which is well known for its good accuracy and moderate time consumption. Moreover, the one-dimensional thermal-hydraulic solver has been added to RAST-F considering properties for FR such as heat capacity, thermal conductivity, viscosity, and density to model the coolant flow in the core. For brevity, the RAST-F notation is used to represent the MCS/RAST-F code system in this paper.

There have been several verification and validation works conducted for RAST-F, with most focusing on k-eigenvalue and depletion calculations [6,10–13]. In the framework of RAST-F developments, a neutron transient module has been implemented in RAST-F at the core level, enabling the prompt and delayed neutron emission models to be simulated. There are many methods to solve the time-dependent neutron balance equation for the transient problem. The point kinetic model with the space-independent approximation has been widely utilized to overcome the cost of computing performance. However, the accuracy of this method is sacrificed in some cases [14–17]. On the other hand, the 3D kinetics equations offer a reasonable way to overcome the limitation of the one-point reactor model and improve the simulation efficiency [18–21]. For that reason, the theta method, precursor integration, and coarse mesh finite difference (CMFD) formulation [22,23] have been implemented in RAST-F to solve the transient fixed source problem. The

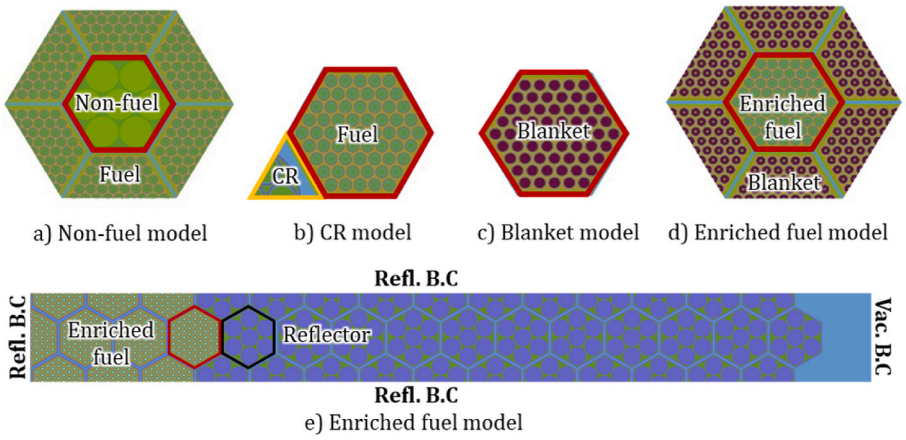

Fig. 2. Sub-assembly models for XS generations.

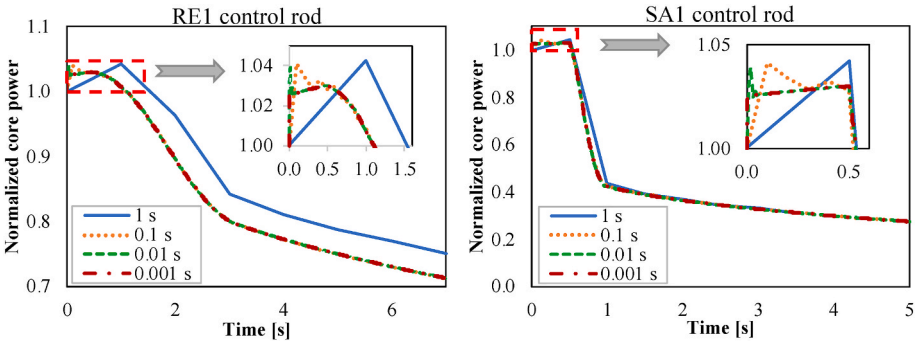

Fig. 3. Impact of time-step size on core power behavior.

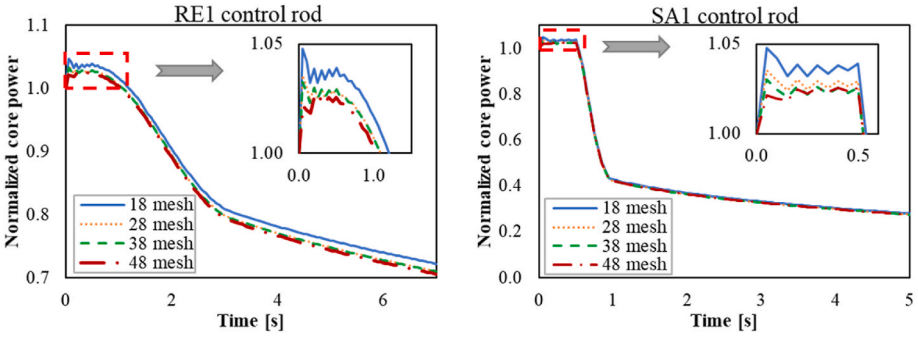

Fig. 4. Impact of fuel axial size on core power behavior.

theoretical calculations and computer modeling of this new implementation need experimental validation for further development.

The proposed CRP based on CEFR experiments provides an excellent opportunity to use RAST-F to validate the transient module while further contributing to the verification and validation of RAST-F analysis capability. According to the CRP, benchmark specification [1] and experimental data were provided to all participating members to validate the codes and nuclear data. However, only a limited number of studies [24,25] have been conducted on these experiments because of the excessive computational costs required for transient whole-core analyses and the complexity of leakage treatments. Nevertheless, these studies focused on simulating the measurements of the control rod worth (CRW) of individual CRs, while the group CRs drop experiments, which were included in the package, were not investigated in these studies. They can introduce a shadowing or anti-shadowing effect. Testing the RAST-F code system on such experiments can demonstrate that the reliability of this code system in time-dependent simulations for FR analysis under the conditions of multiple CR interactions.

In this study, CR drop experiments are simulated using the hybrid code system RAST-F. This study aims to further demonstrate, verify, and validate the capability of RAST-F in analyzing the time behavior in neutron simulations. The RAST-F solution for each individual CR drop is verified against the 3D core MC solution Serpent [26] to ensure that it is a reliable solver for reactor transient problems based on neutron kinetics equations. Then, the rod drop simulation of each individual CR and CR group is carried out and compared against the experimental values to demonstrate the feasibility of the code system for FR time-dependent analysis. The remainder of this paper is organized as follows. Section 2 provides a brief summary of CEFR and CR drop experiments. The computational methodology is presented in Section 3. Section 4 presents the numerical results obtained using RAST-F and compares them with the Serpent solution and experimental data. Section 5 summarizes the results of this study.

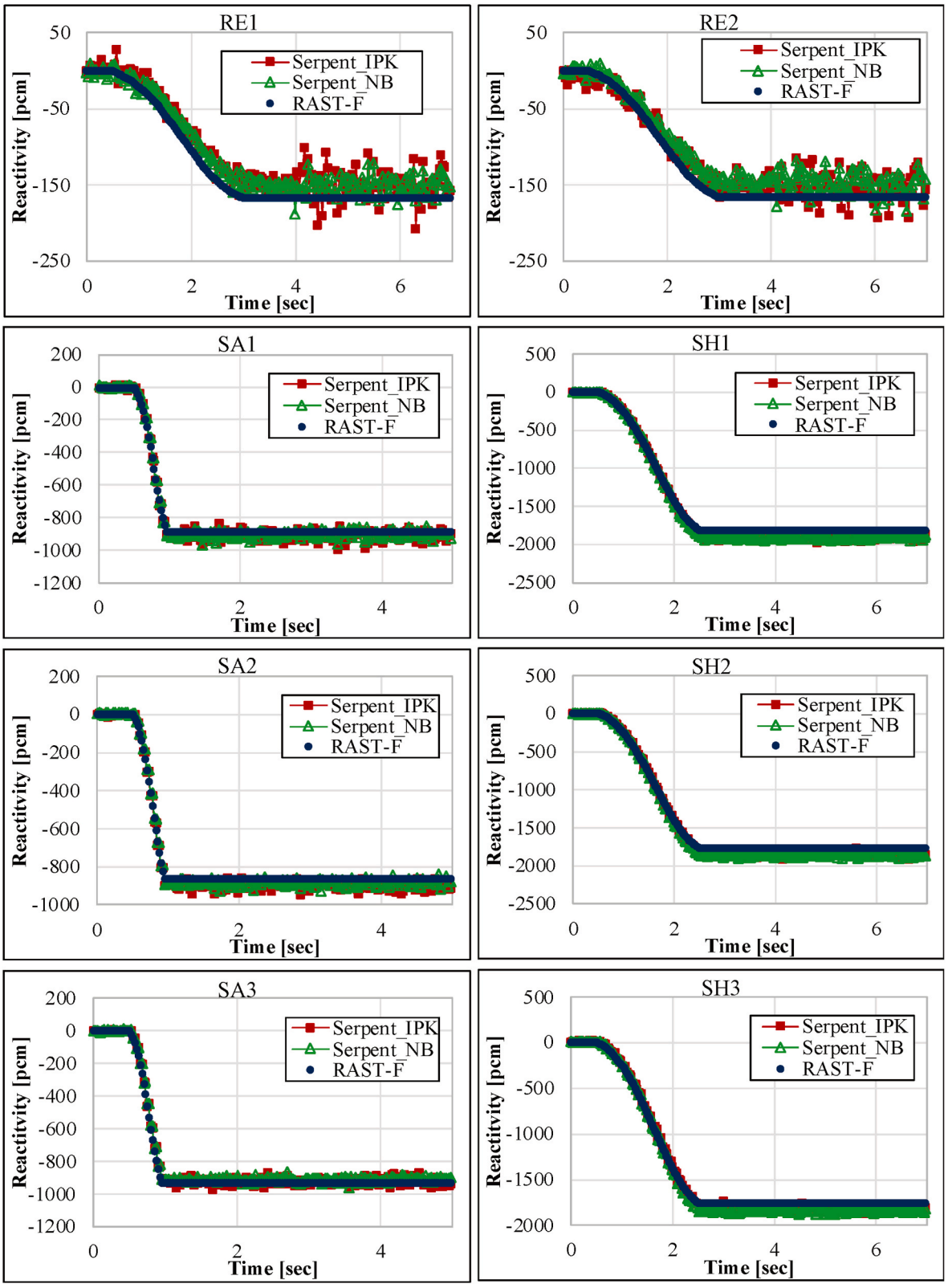

Fig. 5. Time-dependent reactivity calculated via RAST-F and Serpent.

2. Description of the CEFR core and CR drop experiments

The CEFR is a pool-type sodium-cooled FR in China with a thermal power of 65 MW and an electric power of 20 MW. The CEFR reached its first criticality in July 2010. Four experiments were conducted in the physical start-up tests: fuel loading and criticality experiments, measurement of the CRW, measurement of the reactivity coefficients, and foil activation measurements. The physical start-up experiments had three stages: fuel-only loading, operating loading in the cold state, and operating loading in the hot state. In this study, all physical start-up tests

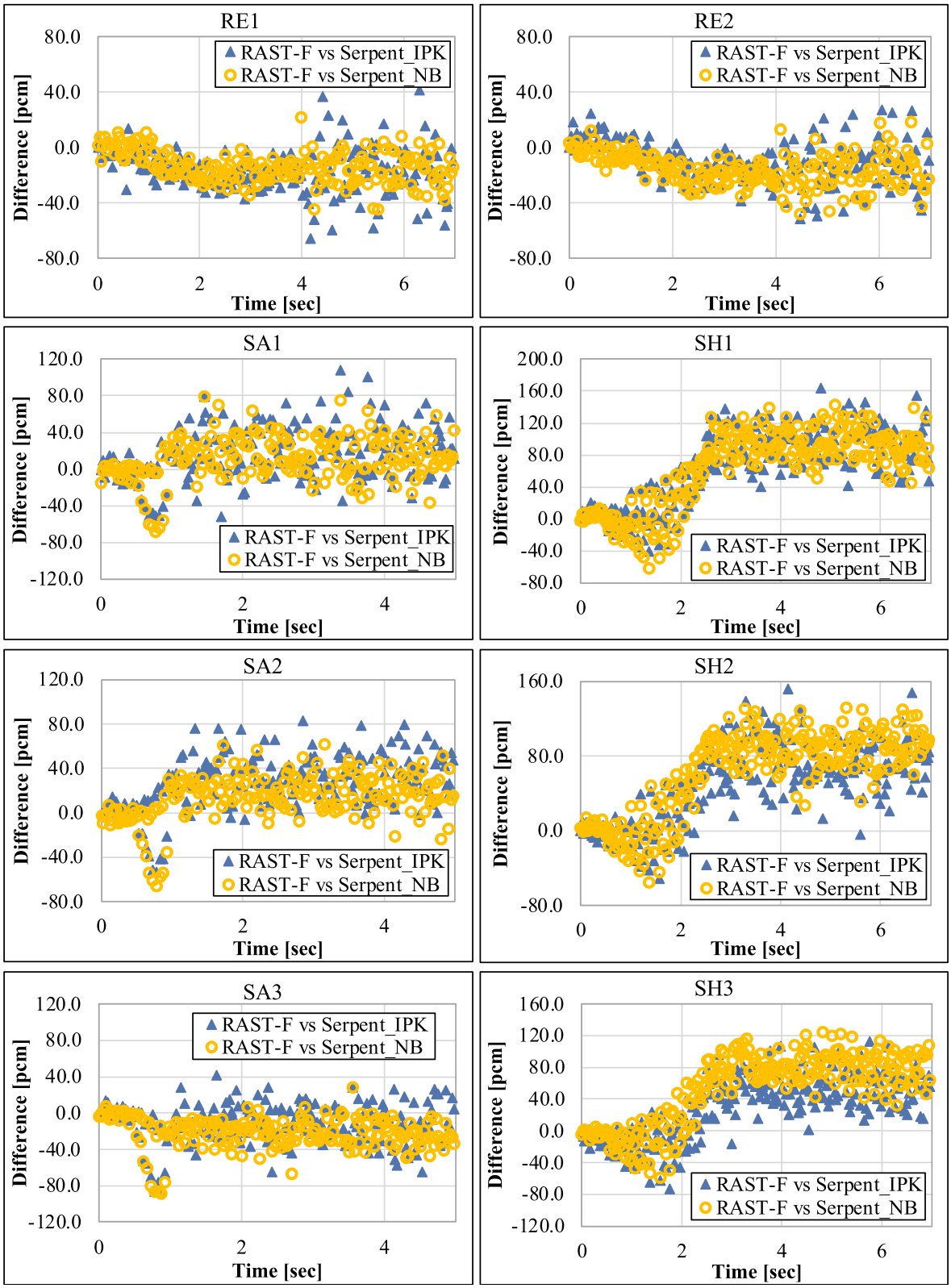

Fig. 6. Comparison of difference in reactivity between RAST-F and Serpent.

were conducted in a cold state (250 °C). The core at the operating loading consisted of 79 fuel sub-assemblies, as illustrated in Fig. 1. The active fuel height of the core was 45 cm. The sub-assembly pitch was 6.1 cm. In addition, the core was loaded with eight controls, one neutron source, 394 stainless steel reflectors, and 230 boron shield sub-assemblies. The core reactivity was controlled by three types of CRs: regulating rods (two sub-assemblies), shim rods (three sub-assemblies), and safety rods (three sub-assemblies). The main difference between the three types of control sub-assemblies is the enrichment of ^{10}B in the B_4C absorber. The enrichments of ^{10}B in regulating (RE), shim (SH), and safety (SA) rods are 19.6 at. % (natural abundance), 92 at. %, and 92 at. %, respectively. Corresponding to the mass of ^{10}B in each control sub-

Table 3
Control rod worth comparison between RAST-F and Serpent.

CRs	RAST-F	Serpent (±1σ)		Absolute diff. [pcm]	
	$\Delta\rho_{RF}$ [pcm]	$\Delta\rho_{IPK}$ [pcm]	$\Delta\rho_{NB}$ [pcm]	RF vs S_{IPK}	RF vs S_{NB}
RE1	166	145 ± 8	150 ± 5	21	15
RE2	165	148 ± 7	138 ± 5	19	27
SH1	1815	1911 ± 7	1918 ± 6	−95	−103
SH2	1770	1848 ± 8	1858 ± 6	−78	−88
SH3	1759	1809 ± 7	1843 ± 6	−50	−84
SA1	885	906 ± 6	911 ± 5	−21	−26
SA2	866	898 ± 4	889 ± 3	−31	−22
SA3	932	925 ± 4	914 ± 3	8	17

assembly, the regulating rod sub-assemblies are used to maintain minor reactivity variation. In contrast, the shim and safety rods are used to compensate for significant reactivity changes and emergency shut-downs, respectively. Detailed descriptions of the geometry, materials, and experiments can be found in Refs. [1,12,13,27,28].

The CRW measurements were obtained in two movement procedures: rod drop and normal-speed movements. Measurements under normal movement were conducted by shifting the measured rod and other rods after each movement to compensate for the reactivity change while maintaining the core at a positive reactivity. Because this process has many varying CR positions, it is extremely time-consuming for neutronic simulation. Therefore, this measurement was excluded from the benchmark.

On the other hand, the measurement by the rod drop is much simpler. Initially, the measured rod was withdrawn to the out-of-core position, and different rods were appropriately altered to maintain a slightly supercritical system. After adjusting the CR positions, the neutron flux increased. The real-time reactivity was obtained from the counting rates measured from source-range detectors. When the count rate from the detector reached a specific number of counts per second, the measurement of the CRW was started, and the measured rod was dropped. The locations of these detectors in the radial view are illustrated in Fig. 1. It is noteworthy that there are 4 positions (4 channels) of source range detectors, situated closely together. During the start-up operation, the neutron flux at out-of-core locations is relatively low. To effectively monitor neutron flux in such situations, boron-lined proportional counters are utilized. These counters offer a high level of neutron sensitivity with the ability to detect up to 30 cps/nv. The CR position during the experiment and insertion speed are listed in Table 1. These detectors were connected to a reactivity meter in the central control room. The reactivity meter recorded the count rate every 0.1 s and calculated the reactivity based on the inverse kinetics method. All kinetic parameters were determined using a deterministic code with ENDF/B-VI, JENDL-3, and CENDL-2 cross-section data for all calculations throughout the start-up experiments. Delayed neutrons were divided into six groups based on the life of the precursor. The decay constants of each group were calculated using the average of all fission nuclides. These parameters tabulated in Table 2. During the measurement process, the rod is dropped once the count rate of detectors reaches 30,000 cps. A fundamental condition is maintained, ensuring that the neutron count rate remains below 35,000 cps. By following this criterion, the reactivity underestimation caused by the dead-time effect is generally kept within 1 pcm [29].

3. Computational methodology and simulation

3.1. Formulation of multi-group CMFD transient fixed source problem

RAST-F is a new full-core analysis nodal code capable of k-eigenvalue, depletion, and thermal-hydraulic calculations, which is under development by the CORE laboratory for FR applications. Several verification and validation works have been carried out for RAST-F, and most have focused on k-eigenvalue and depletion calculations. In the framework of RAST-F development, a neutron time-dependent module has been developed based on the CMFD formulation, theta method [30–32], and a second-order precursor integration technique [32–36]. The theta method and precursor integration technique were adopted to discretize the time-dependent term in the nodal balance equation. The time-dependent nodal balance equations for neutron behavior are given as Eq. (1) with the notations $\overline{\varphi_g^m}$ and C_k^m representing the node average flux and precursor density, respectively, at a computational node m, neutron energy group g, and delay neutron precursor group k:

$$\frac{1}{v_g^m}\frac{d\varphi_g^m}{dt} = R_g^m \equiv \left(1-\sum_{k=1}^{K}\beta_k^m\right)\chi_{pg}\psi^m + \chi_{dg}S_d^m - L_g^m + + \sum_{g'=1}^{G}\Sigma_{g'g}^{m,n}\varphi_g^{m,n} - \Sigma_{t,g}^{m,n}\varphi_g^{m,n} \tag{1}$$

$$\frac{dC_k^m}{dt} = \beta_k^m\psi^m - \lambda_k C_k^m \tag{2}$$

where k_{eff} is the eigenvalue, v_g^m is the neutron velocity, χ_g is the neutron spectrum; $\nu_g\Sigma_{fg}^m$, Σ_{gg}^m, and Σ_{tg}^m are the nu-fission, scattering, and total cross-section, respectively; λ_k is the decay constant; and $J_{gu}^{m\pm}$ is the surface average net current. $\psi^m \equiv \frac{1}{k_{eff}}\sum_{g=1}^{G}\nu\Sigma_{fg}^m\varphi_g^m$, $S_d^m \equiv \sum_{k=1}^{K}\lambda_k C_k^m$, represents total fission, delayed neutron sources, and $L_g^m = \sum_{u=x,y,z}\frac{1}{h_u^m}(J_{g,u}^{m+} - J_{g,u}^{m-})$ represents group leakage.

By applying the theta method to Eq. (1), it can be discretized for a specified time interval $\Delta t_n = t_n - t_{n-1}$ at time point n as follows:

$$\frac{\varphi_g^{m,n} - \varphi_g^{m,n-1}}{v_g^m\Delta t_n} = \theta R_g^{m,n} + (1-\theta)R_g^{m,n-1} \tag{3}$$

where $R_g^{m,n}$ represents for the right-hand-side term of Eq. (1). Eq. (3) can be rewritten as follows:

$$\frac{\varphi_g^{m,n}}{\theta v_g^m\Delta t_n} - R_g^{m,n} = \frac{\varphi_g^{m,n-1}}{\theta v_g^m\Delta t_n} + \overline{\Theta}R_g^{m,n-1} \tag{4}$$

where $\overline{\Theta} = \frac{1}{\theta} - 1$ for $0 < \theta \le 1$. It is assumed that all the parameters at the previous time point are known when solving the problem at time point n. This method can provide second-order accuracy and reliability for a comprehensive time interval when $\theta = 0.5$. Moreover, the accuracy and stabilization can be further improved by applying the theta method after an exponential transform with an appropriate choice of inverse period ($\alpha_g^{m,n}$) for the exponential transformation cases.

$$\left(\frac{1}{\theta v_g^m\Delta t_n} + \frac{\alpha_g^{m,n}}{v_g^m}\right)\varphi_g^{m,n} - R_g^{m,n} = \left[\left(\frac{1}{\theta v_g^m\Delta t_n} - \frac{\overline{\Theta}\alpha_g^{m,n}}{v_g^m}\right)\varphi_g^{m,n-1} + \overline{\Theta}R_g^{m,n-1}\right]e^{\alpha_g^{m,n}\Delta t_n} \tag{5}$$

An unknown that needs to be determined in the R_g term of the balance equation is the delayed neutron source term at time point n. By using the precursor integration technique, the delay source term at time point n can be shifted into the total fission and delayed terms at the previous time point derived from the quadratic fission source variation approximation. By substituting the delayed source term into Eq. (4) and presenting all the parameters, the transient fixed source problem can be expressed as follows:

$$\left(\widetilde{\Sigma}_{r,g}^{m,n} - \left[(1-\beta^m)\chi_{pg} + \omega_n^m\chi_{dg}\right]\lambda\nu\Sigma_f^{m,n}\right)\varphi_g^{m,n} - \sum_{\substack{g'=1 \\ g'\neq g}}^{G}\Sigma_{g'g}^{m,n}\varphi_{g'}^{m,n} + L_g^{m,n} = \chi_{dg}\widetilde{S}_d^{m,n-1} + S_g^{m,n} \tag{6}$$

where

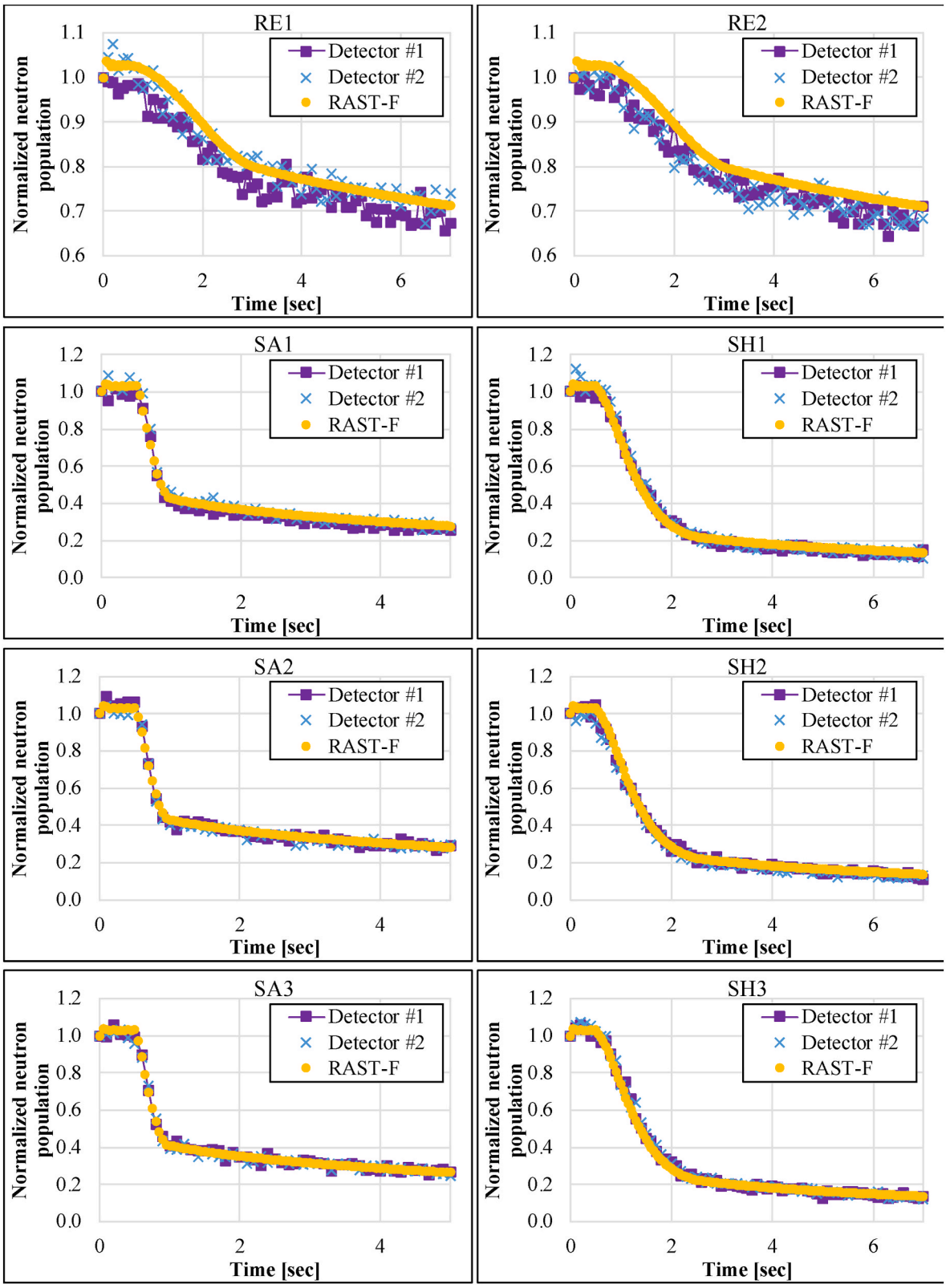

Fig. 7. RAST-F and measured normalized neutron population for individual CR drops.

$$\tilde{\Sigma}_{r,g}^{m,n} \equiv \frac{1}{\theta v_g^m \Delta t_n} + \frac{\alpha_g^{m,n}}{v_g^m} + \Sigma_{rg}^{m,n}, S_g^{m,n}$$
$$\equiv \left[\left(\frac{1}{\theta v_g^m \Delta t_n} - \frac{\overline{\Theta}\alpha_g^{m,n}}{v_g^m} \right) \varphi_g^{m,n-1} + \overline{\Theta} R_g^{m,n-1} \right] e^{\alpha_g^{m,n} \Delta t_n}, \text{ and } \lambda \equiv \frac{1}{k_{eff}}$$

The spatial discretization through the leakage term at time point n can be expressed as Eq. (7) using the node average fluxes and other known factors from the TPEN solutions. Note that the time index is excluded for a concise presentation.

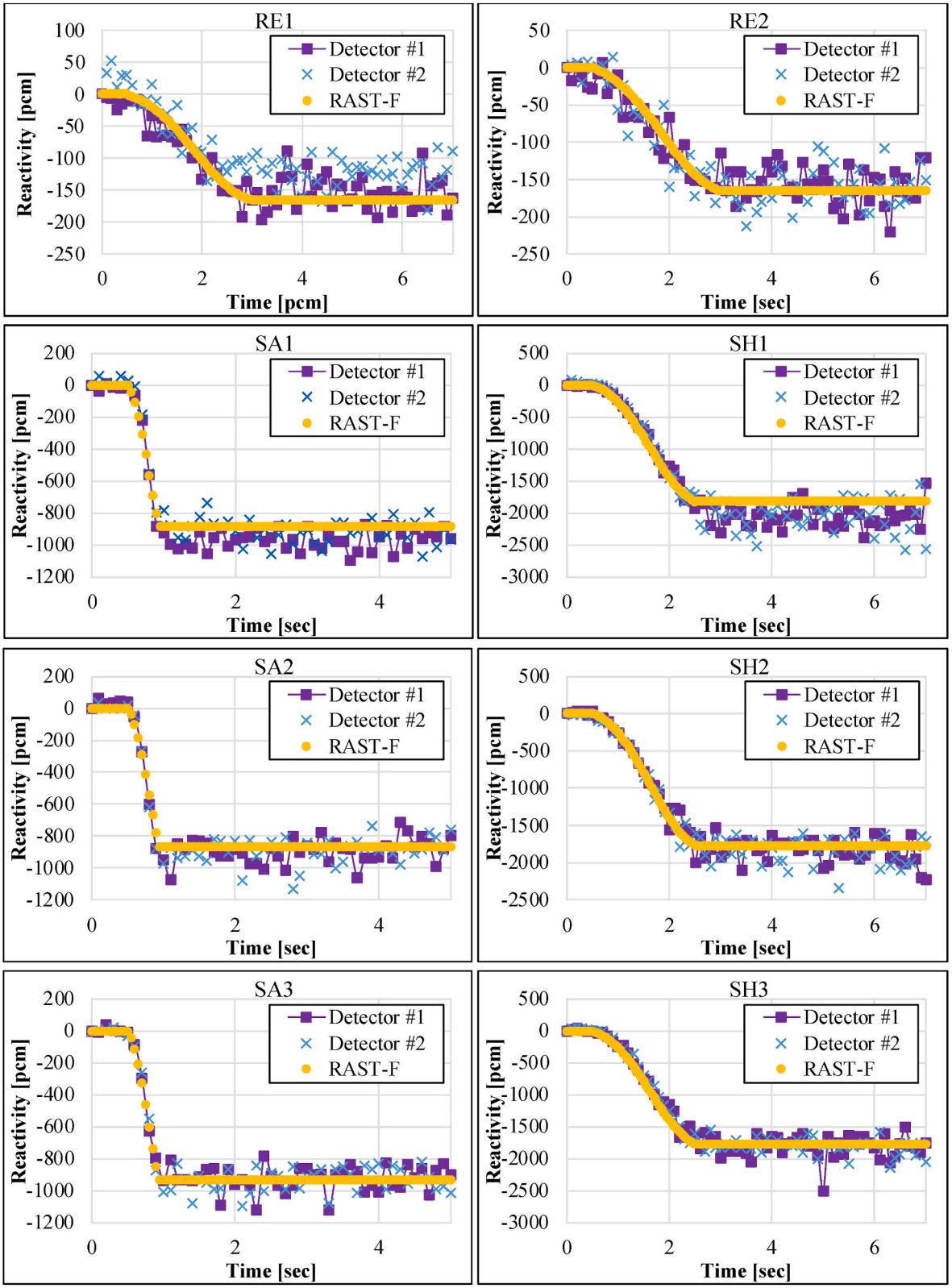

Fig. 8. RAST-F and measured time-dependent reactivity for individual CR drops.

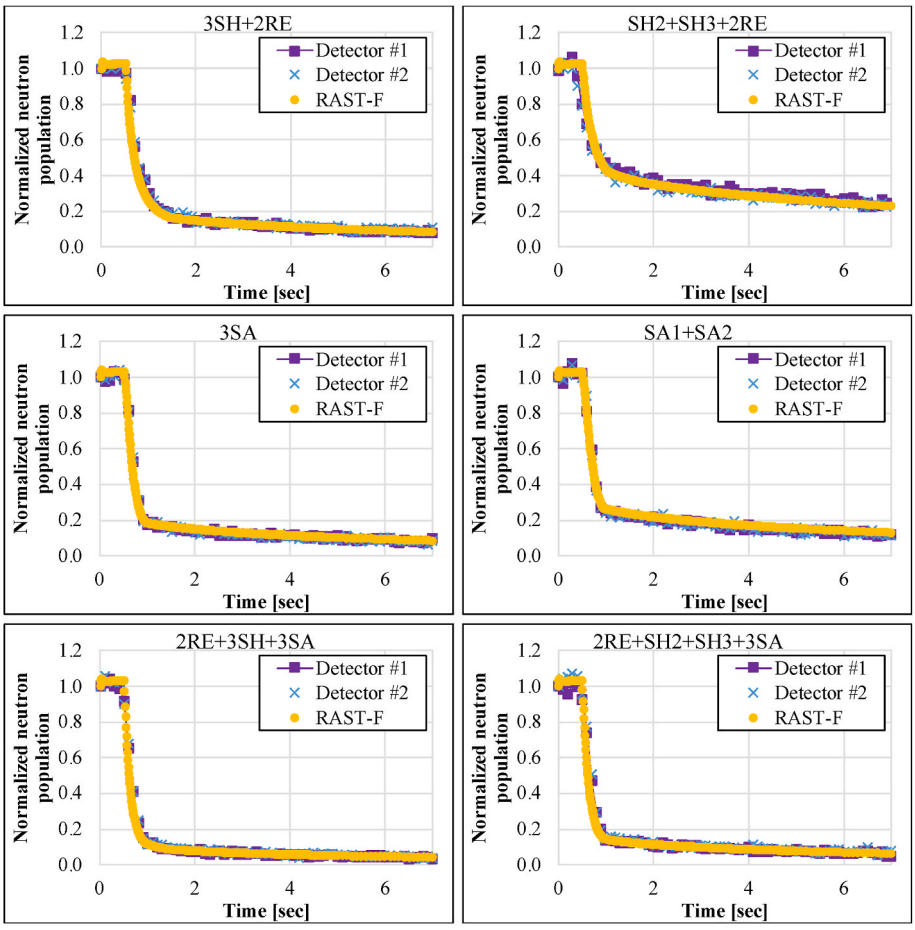

Fig. 9. RAST-F and measured normalized neutron population for CR group drops.

$$J^{m,CMFD}_{g,ud} = -\widetilde{D}^{m}_{g,ud}\left(\varphi^{m}_{g,ud}-\varphi^{m}_{g}\right)-\widehat{D}^{m}_{g,ud}\left(\varphi^{m}_{g,ud}+\varphi^{m}_{g}\right) \quad (7)$$

where $\widetilde{D}^{m}_{g,ud} = \frac{2D^{m}_{g,ud}D^{m}_{g}}{D^{m}_{g,ud}\Delta u_{m}+D^{m}_{g}\Delta u^{ud}_{m}}$, and $\widehat{D}^{m}_{g,ud} = -\frac{\widetilde{D}^{m}_{g,ud}(\varphi^{m}_{g,ud}-\varphi^{m}_{g})+J^{m,nodal}_{g,ud}}{\varphi^{m}_{g,ud}+\varphi^{m}_{g}}$.

The m, u, and d indices are for the nodes, axis, and directions, respectively. Here, $\widetilde{D}^{m\pm}_{gu}$ is the flux difference-to-current conversion factor determined by diffusion coefficients and node size, and $\widehat{D}^{m}_{g,ud}$ is a current correction factor that can be determined from the nodal calculation (TPEN solution). Substituting Eq. (7) into the leakage term in Eq. (1), the solution of the fixed source problem can be presented in a linear system form with only one unknown: node average flux.

3.2. XS generation and core model

The XS generation code MCS and ENDF/B-VII.1 nuclear data files [37] were used to prepare multi-group XSs for the nodal calculation. The spectral effect in the CEFR was revealed in Ref. (13), which caused a massive challenge for nodal analysis tools. Significant deviations were observed in a common approach for fuel XS generation, which is a 2D single fuel sub-assembly model with reflective boundary conditions. This difficulty was resolved using the fuel-blanket model to reproduce the spectrum of the fuel sub-assembly in the active core to provide homogenized few-group constants. The same approach is adopted for XS generation in this study as follows:

- The XS for the non-fuel region was generated using a 2D supercell model (as in Fig. 2a). The non-fuel hexagonal region is located in the center and surrounded by six HEU fuel sub-assemblies. The boundary conditions were reflective in the axial and radial directions.
- The XS for the absorber region in the control sub-assembly and nearby fuel region was prepared using a 2D supercell model (as in Fig. 2b). The super-homogenization (SPH) method was applied to correct the XSs in the case of the control sub-assembly shift.
- The XS for the blanket region was generated using a 2D single model (as in Fig. 2c). The XS for the HEU fuel region was generated using a 2D supercell model (as in Fig. 2d). The boundary conditions were reflective in the axial and radial directions.
- The 2D fuel-reflector model was used to generate XS for the most outer HEU fuel and nearby radial reflector regions with an axial reflective boundary condition, as shown in Fig. 2e.

Owing to the high statistical uncertainty in the thermal energy ranges when using the MC code, the homogenized group constant data were generated based on a 24-group energy structure [38]. XS generation was simulated with a total of 12 million neutron histories, including 100/20 cycles (active/skipped) and 100,000 neutron histories per cycle for all MC code simulations. The SPH factors [39] were applied for the control and adjacent fuel sub-assemblies when the control sub-assembly was inserted into the active core region. To achieve precise calculations, a fine axial mesh will be utilized in this paper. The fine mesh offers the advantage of implementing a simple volume homogenization technique, which effectively preserves the volume and mass of the control sub-assemblies, even when it falls between the boundaries of an axial mesh.

In the 3D core simulation, the RAST-F calculation was performed at an initial zero-power state without thermal-hydraulic feedback. Thermal expansion was considered in both the axial and radial directions.

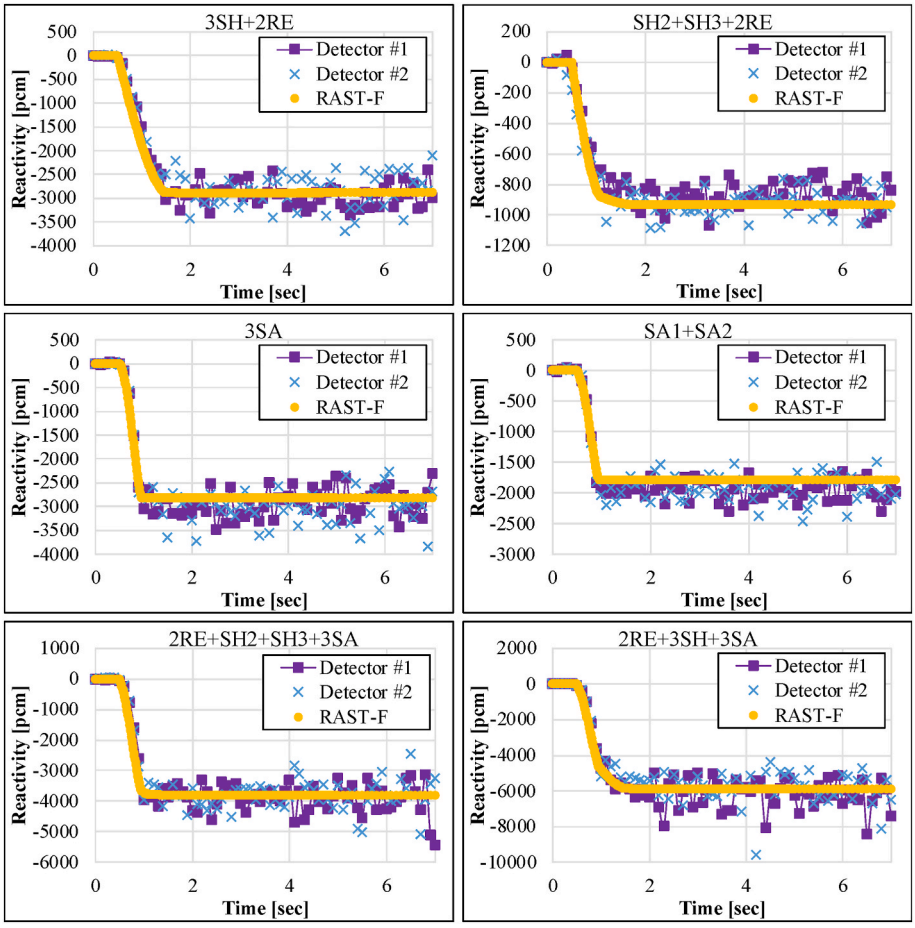

Fig. 10. RAST-F and measured time-dependent reactivity for CR group drops.

Table 4
Control rod worth comparison between RAST-F and measurement data for individual CR drops.

CRs	RAST-F	Measurement (±1σ)	Absolute diff. [pcm]
	$\Delta\rho_{RF}$ [pcm]	$\Delta\rho_{Mea}$ [pcm]	
RE1	166	150 ± 9	16
RE2	165	149 ± 9	16
SH1	1815	2019 ± 250	−204
SH2	1770	1839 ± 225	−69
SH3	1759	1839 ± 226	−80
SA1	885	945 ± 100	−60
SA2	866	911 ± 100	−45
SA3	932	946 ± 98	−14

Table 5
Control rod worth comparison between RAST-F and measurement data for CR group drops.

CR group	RAST-F	Measurement (±1σ)	Absolute diff. [pcm]
	$\Delta\rho_{RF}$ [pcm]	$\Delta\rho_{Mea}$ [pcm]	
3 × SH+2 × RE	2895	2877 ± 335	18
SH2+SH3+2 × RE	929	881 ± 76	48
3 × SA	2810	2981 ± 395	−171
SA1+SA2	1788	1950 ± 226	−162
2 × RE+3 × SH+3 × SA	5870	6079 ± 989	−209
2 × RE + SH2+SH3+3 × SA	3797	3899 ± 551	−102

The rod-drop simulation was performed using the XS generated by MCS, delayed neutron spectrum from Serpent code, and point kinetic data provided by CIAE. The transient calculation in RAST-F begins with the eigenvalue calculation at the initial state condition to produce and initialize the initial conditions for the transient calculation. These conditions include k_{eff}, flux distribution, corrective nodal coupling coefficients, and precursor densities. The transient simulation is then performed by solving the transient fixed-source problem at the first time point, which is repeated at each subsequent time step. The CR position is updated according to each time step until the rod reaches the rodded position with the corresponding speed listed in Table 1. The dynamic reactivity from CR insertion at time point t is calculated as follows:

$$\rho_{CR} = \frac{\langle \varphi_0^*, A_{CR}\varphi \rangle}{\langle \varphi_0^*, F\varphi \rangle} \tag{8}$$

where $A = F - M$ is the net production operator, F is the fission term, M is all non-fission terms, φ_0^* is adjoint flux from the steady state adjoint calculation, and φ is time-dependent shape functions that can be obtained from spatial kinetics calculation. The subscript CR denotes the control rod.

4. Numerical results

4.1. Sensitivity test

As mentioned in the previous section, the theta method with exponential form and CMFD relation was applied for temporal and spatial discretization, which enables the provision of an efficient and precise transient solution. Therefore, the sensitivities of the transient core

power according to variations in the fuel node and time interval sizes are reviewed in this section. For brevity, only the RE1 and SA1 CRs were used for evaluation. The impact of the time-step size is evaluated based on the overall behavior of the core power during the RE1 and SA1 CRs drop calculations, as shown in Fig. 3. The time-step size is 1 s, 0.1 s, 0.01 s, and 0.001 s. Results with a time step size of 0.001 s can be used as a reference. As the time step size decreases, the core power peaks early in the RE1 and SA1 cases. The core power behavior in the RE1 case with 1 s shows a significant shift compared to the case with 0.001 s, whereas the results of the RE1 rod using 0.1 s and 0.01 s match well compared with those using 0.001 s. Excluding the slight discrepancy in the results using 1 s, other results show good agreement compared with the reference in the SA1 rod calculation.

After optimizing the time step size of the theta method, a sensitivity test regarding the effect of fuel axial mesh on core power behavior was conducted and is shown in Fig. 4. The 3D core transient calculations were conducted with 18, 28, 38, and 48 mesh cases. The time step size is selected as 0.05 s. The results of using 48 meshes were used as a reference. A comparison of the RE1 core power behavior shows a lower peak as the number of meshes increases. Only a slight overestimation was observed in the results of using 18 meshes, and all other results showed excellent agreement with the reference. A lower peak, as the number of meshes increased, was observed in the SA1 power behavior. Nevertheless, the discrepancy is negligible in all cases. Therefore, the transient simulation with 28 axial fuel meshes and 0.05 s of time interval size is sufficient to ensure reliable solutions.

4.2. Verification

To verify the time-dependent diffusion solver, the RAST-F solution was compared against the Serpent solutions [24] using the inverse point kinetics (IPK) method and the time-dependent global neutron balance (NB) to confirm the neutronic performance. There is no information about the Serpent criticality set and standard deviations of the time-dependent neutron population and reactivity. Serpent simulation utilizes JEFF-3.1 based cross-section data. For consistency, the same transient simulation between RAST-F and Serpent was modeled. The absorber rods begin to drop horizontally at 0.5 s with a constant velocity, as listed in Table 1. The simulated transient used a fixed time-step size of 35 ms for RE rods, 28 ms for SH rods, and 25 ms for SA rods. The total simulation time is followed until 7.0 s for RE and SH rods and until 5.0 s for SA rods. The transient reactivity calculated by RAST-F is plotted along with the Serpent solution-calculated NB- and IPK-based reactivities shown in Fig. 5. Generally, the reactivity curves obtained by the RAST-F and Serpent solutions agree well for all cases during the entire simulated time interval. The difference between the RAST-F and Serpent solutions is shown in Fig. 6. Note that the difference has a general behavior; RAST-F progressively underestimates the reactivity from the initial position to around the middle of the active core and gradually shifts to overestimates until the end. As listed in Table 2, the immovable CRs during the measurements were located near the center of the core. Therefore, the measured CRs are weakened in this region owing to the shadowing effect. RAST-F overestimates this effect in comparison to Serpent. This may be caused by the SPH scheme in RAST-F, which propagates the flux depreciation in the vicinity of the immovable CRs, thus affecting the worth of measured CR.

To obtain the dynamic CRW, the linear fit function (LINEST) was used to estimate the worth and its standard deviation. The dynamic CRW was acquired by a linear fitting in reactivity after the CR drop, from 3 s to 7 s for RE rods, from 2.5 s to 7 s for SH rods, and from 0.95 s to 5 s for SA rods. For the CRW, the RAST-F and Serpent results are summarized and compared in Table 3. The RF, S_{IPK}, and S_{NB} notations listed in Table 3 represent RAST-F, Serpent using the IPK method, and Serpent using the NB method, respectively. All RAST-F results generally showed good agreement with the Serpent results, excluding a remarkable discrepancy observed in the regulating CRs with a relative deviation compared to the Serpent values of up to 19.6%. These deviations can be attributed to the kinetic schemes and differences in steady state neutronic approaches.

4.3. Validation

The verification results demonstrate an excellent agreement between the MC and nodal diffusion solutions. In this section, the calculations performed with RAST-F are summarized and compared with the experimental data obtained from the two out-core detectors. The normalized neutron populations, real-time core reactivity, and CRW obtained from these detectors during all individual CR and control group drop experiments were compared to the results obtained from the RAST-F code.

It should be noted that the CR drop experiments were conducted through the ex-core detectors. However, the ex-core detectors are situated at distances exceeding 550 cm from the core center and more than 150 cm from the reactor vessel. Due to these considerable distances, simulating these detectors poses a notable challenge as they are located far from the core center and outside of the reactor vessel. Therefore, this study focuses on conducting the core transient caused by rod drop using RAST-F through 3D space-time kinetics calculation. For individual CR drop experiments, the neutron populations obtained with RAST-F were compared with the measured values and are shown in Fig. 7. The RAST-F solutions from the rod drop simulation exhibit a good agreement with the experimental neutron population for most cases, with the exception of the RE rods. Regarding the core reactivity, a comparison of RAST-F and measurement data is plotted in Fig. 8. A slight discrepancy in reactivity was observed in both RE rods. Because the RE rods are located outside the core region and use the natural ^{10}B absorber to maintain reactivity, the effect of these rods on core reactivity is small but sensitive [13,24,26]. However, good agreement is observed between the RAST-F computational results and measured results for all remaining cases at all simulation times. For the CR group experiments, the CR drop simulations start at 0.5 s and apply the same drop speed for each individual rod, as listed in Table 1. A fixed time step size of 10 ms was used until 7 s for all CR group simulations. The normalized neutron population and time-dependent reactivity simulation solutions are compared to experimental data and shown in Figs. 9 and 10, respectively. Therefore, all the presented cases show good agreement between the deterministic and measurement results during the entire simulation time.

To obtain the dynamic CRW, the same data used in the verification section is utilized for individual CR, while the worth for group CR is obtained with the calculated reactivity from 1.5 s to 7 s using the same function (LINEST) as the verification section. The CRW of each CR is summarized and compared in Table 4. A remarkable discrepancy in the CRW was observed for the SH1 rod with a deviation compared to the experimental values of up to 204 pcm. The underestimation of SH1 CRW can be, indeed, partially explained by a violation of the one-point kinetics theory. The simulation treated the core transient as a comprehensive representation of the entire core's behavior. In contrast, the experimental approach relied on ex-core detectors, which are known to be more sensitive to localized neutron behavior at the core periphery.

The active core region is surrounded by thick shielding subassemblies, with the exception of the side facing ex-core detectors. This specific core configuration significantly diminishes the contribution of the side not facing the detectors to the neutron population measured by the detectors. As a result, the detector signal is mainly generated by the peripheral fuel sub-assemblies located near the detectors. Indeed, the SH1 rod is positioned on the centerline of the detectors, located in the peripheral fuel area directly facing the detectors. Consequently, when the SH1 rod is dropped into the core, a significant localized suppression of neutron population occurs in this peripheral area. The main neutron source's contribution to the detector's signals is directly affected. This results in a higher variation in the neutron

population detected by the detectors during the SH1 drop compared to the variation in the whole core neutron population in the simulation. Consequently, this can lead to a higher experimental CRW for the SH1 rod. The previous study utilizing Serpent has demonstrated this effect on the SH1 CRW [24]. Moreover, the discrepancy may partially be attributed to the use of different approaches for reactivity calculation. The experiment employed a one-point reactor model based on the inverse kinetics equation, assuming a constant neutron flux distribution shape during the dynamic measurement. However, during large reactivity insertions like the SH1 rod, the neutron flux distribution undergoes significant changes throughout the dynamic process. On the other hand, RAST-F employs 3D space-time kinetics theory for dynamic reactivity calculations, allowing the consideration of the changing flux shape during the rod drop process by solving spatial kinetics problems. In general, the calculated results agree with the experimental values within one sigma. The difference in RE rods is up to 16 pcm, which lies within two sigmas of the experimental uncertainty. All the remaining cases agree well with the experimental values within one sigma. It should be noted that the CRW uncertainty includes the uncertainty of both the enrichment of ^{10}B and the density of boron carbide, as well as the uncertainty arising from nuclear data.

The experimental and RAST-F CRWs of all groups are listed in Table 5. Compared to the experimental data, the RAST-F slightly overestimated up to 50 pcm for the worth of 1st shutdown system and the worth of 1st shutdown system with SH1 stuck, whereas all remaining calculated results overestimated the experimental data up to 210 pcm. However, all discrepancies are less than one sigma of the measurement error..

5. Conclusions

In this study, the transient capability of the RAST-F hybrid code system was examined by performing CR drop simulations of real-life CEFR experiments. Homogenized XS and delay neutron spectra were generated by MC codes for the RAST-F simulation. Point kinetic parameters from a deterministic code were included in the benchmark package. The sensitivities in the transient core power according to the variations in the axial fuel mesh and time interval size were investigated to obtain a trustworthy result and lower computational cost. The parameters of interest, including the normalized neutron population, dynamic reactivity, and CRW of eight individual CRs and six CR groups, were computed using the multi-group CMFD transient solver in RAST-F. The calculated results of RAST-F were compared with the MC solution of all individual CRs and validated against the measurement data of all eight individual CRs and six CR groups.

The investigation on the axial fuel mesh and time interval size proved that the multi-group CMFD transient solver in RAST-F is stable and reliable to provide an accurate solution for CEFR transient simulation with 28 axial fuel meshes and 0.1 s of time interval size. For comparison with the Serpent solution, the time-dependent reactivity and CRW obtained by RAST-F show good agreement. A significant discrepancy was observed in the SH1 rod drop simulation. However, the difference is smaller than 160 pcm compared to the Serpent data. These deviations can be attributed to the kinetic schemes and differences in steady state neutronic approaches. Compared with the data obtained from the experiment, the RAST-F solution is almost identical to the measurement data in terms of neutron population and reactivity. All calculated CRW results agreed with the experimental results within two sigmas of experimental uncertainty for all CRs and CR groups comparisons.

Therefore, the transient capability was successfully tested against the CEFR experiments, indicating that the RAST-F code system can be used for FR transient analysis under the conditions of multiple CRs interactions. In addition, this study contributes to validating the RAST-F code system for neutronic core analysis. However, note that the experimental results were obtained from out-of-core detectors, which was not conducted in this study. In the future, a precise simulation of the detector response should be obtained for further validation. Moreover, uncertainty quantification and sensitivity analysis with the RAST-F code system should be investigated.

Declaration of competing interest

The authors declare that they have no known competing financial interests or personal relationships that could have appeared to influence the work reported in this paper.

Acknowledgments

This work was partially supported by the National Research Foundation of Korea (NRF) grant funded by the Korea government (MSIT). (No. NRF-2019M2D2A1A03058371).

This research was partially supported by the project (L20S089000) by Korea Hydro & Nuclear Power Co. Ltd.

This work was partially supported by Korea Institute of Energy Technology Evaluation and Planning (KETEP) grant funded by the Korea government (MOTIE) [RS-2023-00241302].

The data and information presented in the paper are part of an ongoing IAEA coordinated research project on "Neutronics Benchmark of CEFR Start-Up Tests – CRP-I31032".

References

[1] X. Huo, et al., Technical Specifications for Neutronics Benchmark of CEFR Start-Up Tests, China Institute of Atomic Energy, 2019. IAEA CRP-I31032.
[2] S. Choi, et al., Development of high-Fidelity neutron transport code STREAM, Comput. Phys. Commun. 264 (2021), 107915.
[3] J. Jang, S. Dzianisau, D. Lee, Development of nodal diffusion code RAST-V for vodo-vodyanoi Energetichesky reactor analysis, Nucl. Eng. Technol. 54 (2022) 3494–3515.
[4] J. Jang, et al., Analysis of rostov-II benchmark using conventional two-step code systems, Energies 15 (2022) 3318.
[5] T.Q. Tran, A. Cherezov, X. Du, D. Lee, Verification of a two-step code system MCS/RAST-F to fast reactor core analysis, Nucl. Eng. Technol. 54 (2022) 1789–1803.
[6] T.D.C. Nguyen, H. Lee, D. Lee, Use of Monte Carlo code MCS for multigroup cross section generation for fast reactor analysis, Nucl. Eng. Technol. 53 (2021) 2788–2802.
[7] J.Y. Cho, C.H. Kim, Higher order polynomial expansion nodal method for hexagonal core neutronics analysis, Ann. Nucl. Eng. 25 (1998) 1021–1031.
[8] J.Y. Cho, et al., Hexagonal CMFD formulation employing triangle-based polynomial expansion nodal kernel, in: International Conference on Mathematics and Computational Methods Applied to Nuclear Science and Engineering (M&C), 2001. Salt Lake City, Utah, USA, September 9.
[9] M. Pusa, Rational approximations to the matrix exponential in burnup calculations, Nucl. Sci. Eng. 169 (2011) 155–167.
[10] T.Q. Tran, A. Cherezov, X. Du, J. Park, D. Lee, Development of hexagonal-Z geometry capability in RAST-K for fast reactor analysis, in: International Conference on Emerging Nuclear Energy Systems (ICENES), 2019. Bali, Indonesia, October 6-9.
[11] T.Q. Tran, S. Dzianisau, T.D.C. Nguyen, D. Lee, Verification of a depletion solver in RAST-K for fast reactor analysis, in: Korean Nuclear Society Virtual Autumn Meeting, 2020. R. Korea, Dec 16-18.
[12] T.Q. Tran, T.D.C. Nguyen, D. Lee, CEFR simulation using diffusion code system RAST-F, in: International Conference on Physics of Reactors (PHYSOR), 2022. Pittsburgh, USA, May 15-20.
[13] T.Q. Tran, D. Lee, Neutronic simulation of the CEFR experiments with the nodal diffusion code system RAST-F, Nucl. Eng. Technol. 54 (2022) 2635–2649.
[14] J. Yasinsky, A. Henry, Some numerical experiments concerning space-time reactor kinetics behavior, Nucl. Sci. Eng. 22 (1965) 171–181.
[15] J.P. Hamric, Spatial kinetics in large reactors, Trans. Am. Nucl. Soc. 8 (1965).
[16] Y. Chao, A. Attard, A resolution to the stiffness problem of reactor kinetics, Nucl. Sci. Eng. 90 (1985) 40–46.
[17] J. Sanchez, On the numerical solution of the point kinetics equations by generalized Runge-Kutta methods, Nucl. Sci. Eng. 103 (1989) 94–99.
[18] D.A. Meneley, K. Ott, E.S. Wiener, Space-Time Kinetics-The QX-1 Code, Argonne National Laboratory, 1968. ANL-7310.
[19] D.A. Meneley, K. Ott, E.S. Wiener, Fast Reactor Kinetics-The QX-1 Code, Argonne National Laboratory, 1971. ANL-7769.
[20] S.K. Chae, Review of computational methods for space-time reactor kinetics, J. Korean Nucl. Soc. 11 (1979) 219–229.
[21] T.M. Sutton, B.N. Aviles, Diffusion theory methods for spatial kinetics calculations, Prog. Nucl. Eng. 30 (1996) 119–182.
[22] T. Downar, et al., PARCS v3.0 U.S. NRC Core Neutronics Simulator Theory Manual, University of Michigan, USA, 2010.

[23] Y.A. Chao, Coarse mesh finite difference methods and applications, in: International Conference on Physics of Reactors, PHYSOR), Pittsburgh, Pennsylvania, USA, 2000. May 7-12.
[24] E. Fridman, X. Huo, Dynamic simulation of the CEFR control rod drop experiments with the Monte Carlo code Serpent, Ann. Nucl. Eng. 148 (2020), 107707.
[25] I. Pataki, et al., Validation of the KIKO3DMG neutronics code on the CEFR start-up tests, Ann. Nucl. Eng. 180 (2023), 109493.
[26] J. Leppänen, M. Pusa, T. Viitanen, V. Valtavirta, T. Kaltiaisenaho, The Serpent Monte Carlo code: status, development and applications in 2013, Ann. Nucl. Eng. 82 (2015) 142–150.
[27] X. Du, J. Choe, T.Q. Tuan, D. Lee, Neutronic simulation of China Experimental Fast Reactor start-up tests. Part I: SARAX code deterministic calculation, Ann. Nucl. Eng. 136 (2020), 107046.
[28] T.Q. Tran, J. Choe, X. Du, H. Lee, D. Lee, Neutronic simulation of China experimental fast reactor start-up tests part II: MCS code Monte Carlo calculation, Ann. Nucl. Eng. 148 (2020), 107710.
[29] Y. Hu, Y. Zhao, X. Chen, L. Xu, Proposing of a new fitting and iteration method (FIM) to correct measured reactor core reactivity, Nucl. Eng. Des. 254 (2013) 33–42.
[30] A.F. Henry, A.V. Vota, WIGL2-A Program for the Solution of the One-Dimensional, Two-Group, Space-Time Diffusion Equations Accounting for Temperature, Xenon, and Control Feedback, Bettis Atomic Power Lab., 1965. WAPD-TM-532.
[31] J.B. Yasinsky, M. Natelson, L.A. Hageman, TWIGL-A Program to Solve the Two-Dimensional, Two-Group, Space-Time Neutron Diffusion Equations with Temperature Feedback, Bettis Atomic Power Lab., 1968. WAPD-TM-743.
[32] W.M. Stacey, Space-time Nuclear Reactor Kinetics, Academic Press, New York, 1969.
[33] K.F. Hansen, et al., GAKIN: a One Dimensional Multigroup Kinetics Code, Calif. General Atomic Div., 1967. GA-7543.
[34] W.T. McCormick Jr., K.F. Hansen, Numerical Solution of the Two-Dimensional Time-dependent Multigroup Equations, Massachusetts Institute of Technology, 1969. MIT-3903-1.
[35] K.F. Hansen, J.H. Mason, GAKIN II : a One-Dimensional Multigroup Diffusion Theory Reactor Kinetics Code, Massachusetts Institute of Technology, 1973. COO-2262-3.
[36] A.L. Wight, K.F. Hansen, D.R. Ferguson, Application on alternating-direction implicit methods to the space-dependent kinetics equations, Nucl. Sci. Eng. 44 (1971) 239–251.
[37] M.B. Chadwick, et al., ENDF/B-VII.1 nuclear data for science and Technology: cross sections, covariances, fission product yields and decay data, Nucl. Data Sheets 112 (2011) 2887–2996.
[38] E. Fridman, E. Shwageraus, Modeling of SFR cores with serpent-DYN3D codes sequence, Ann. Nucl. Eng. 53 (2013) 354–363.
[39] A. Kavenoky, The SPH homogenization method, in: Specialists' Meeting on Homogenization Methods in Reactor Physics, Lugano, Switzerland, 1978. November 13-15.